Published in final edited form as:
Neurobiol Dis. 2013 January ; 0: 211–220. doi:10.1016/j.nbd.2012.08.012.

Preferential inactivation of *Scn1a* in parvalbumin interneurons increases seizure susceptibility

Stacey B. Dutton[1], **Christopher D. Makinson**[1], **Ligia A. Papale**[1], **Anupama Shankar**[1], **Bindu Balakrishnan**[1], **Kazu Nakazawa**[2], and **Andrew Escayg**[1]

[1]Department of Human Genetics, Emory University, Atlanta, GA, 30022

[2]Unit on Genetics of Cognition and Behavior, National Institute of Mental Health, Bethesda, MD

Abstract

Voltage-gated sodium channels (VGSCs) are essential for the generation and propagation of action potentials in electrically excitable cells. Dominant mutations in *SCN1A*, which encodes the $Na_v1.1$ VGSC α-subunit, underlie several forms of epilepsy, including Dravet syndrome (DS) and genetic epilepsy with febrile seizures plus (GEFS+). Electrophysiological analyses of DS and GEFS+ mouse models have led to the hypothesis that *SCN1A* mutations reduce the excitability of inhibitory cortical and hippocampal interneurons. To more directly examine the relative contribution of inhibitory interneurons and excitatory pyramidal cells to *SCN1A*-derived epilepsy, we first compared the expression of $Na_v1.1$ in inhibitory parvalbumin (PV) interneurons and excitatory neurons from P22 mice using fluorescent immunohistochemistry. In the hippocampus and neocortex, 69% of $Na_v1.1$ immunoreactive neurons were also positive for PV. In contrast, 13% and 5% of $Na_v1.1$ positive cells in the hippocampus and neocortex, respectively, were found to co-localize with excitatory cells identified by *CaMK2α* immunoreactivity. Next, we reduced the expression of *Scn1a* in either a subset of interneurons (mainly PV interneurons) or excitatory cells by crossing mice heterozygous for a floxed *Scn1a* allele to either the *Ppp1r2-Cre* or *EMX1-Cre* transgenic lines, respectively. The inactivation of one *Scn1a* allele in interneurons of the neocortex and hippocampus was sufficient to reduce thresholds to flurothyl- and hyperthermia-induced seizures, whereas thresholds were unaltered following inactivation in excitatory cells. Reduced interneuron *Scn1a* expression also resulted in the generation of spontaneous seizures. These findings provide direct evidence for an important role of PV interneurons in the pathogenesis of *Scn1a*-derived epilepsies.

Keywords

Epilepsy; *SCN1A*; ion channels; interneurons; pyramidal neurons

Corresponding Author: Andrew Escayg, Ph.D., Emory University, Department of Human Genetics, 615 Michael Street, Whitehead Building, Suite 301, Atlanta, Georgia 30322, USA, Telephone number: (404) 712-8328, Fax number: (404) 727-3949, aescayg@emory.edu.

Introduction

Mutations in the voltage-gated sodium channel (VGSC) *SCN1A*, which encodes the α-subunit of $Na_v1.1$ channels, are responsible for several epilepsy subtypes, including Dravet syndrome (DS) and genetic epilepsy with febrile seizures plus (GEFS+)(Escayg et al., 2000; Claes et al., 2001). Loss-of-function *SCN1A* mutations cause DS, a debilitating form of epilepsy characterized by complex febrile seizures in the first year of life, partial and/or generalized afebrile epilepsy, intellectual disability, and ataxia (reviewed in Catterall et al., 2010; Escayg & Goldin, 2010). Mutations that cause GEFS+, on the other hand, typically alter the biophysical properties of $Na_v1.1$ channels. GEFS+ is often characterized by febrile seizures that persist beyond six years of age and epilepsy in adulthood (reviewed in Escayg & Goldin, 2010). In addition, a spectrum of seizure types and severities are often observed among affected members of GEFS+ families, as well as between different families (Grant & Vazquez, 2005; Barela et al., 2006; Mahoney et al., 2009).

Emerging data from mouse models of DS and GEFS+ are beginning to provide insight into disease mechanisms. Electrophysiological analyses of dissociated hippocampal and cortical interneurons from *Scn1a* knockout mice or mice carrying a human *SCN1A* nonsense mutation (models of DS) revealed reduced sodium currents and cell excitability (Yu et al., 2006; Ogiwara et al., 2007). In contrast, sodium currents are unaltered in pyramidal cells. A role for reduced interneuron excitability in *SCN1A*-derived epilepsy has also been inferred by electrophysiological data from transgenic and knock-in models expressing the human *SCN1A* GEFS+ mutation R1648H (Tang et al., 2009; Martin et al., 2010).

Interneurons comprise a highly heterogeneous population of cells that differ in their morphological, functional, and molecular characteristics. Although the expression of *SCN1A* among interneuron cell-types has not been fully characterized, Ogiwara et al. (2007) reported that the majority of parvalbumin-positive (PV) interneurons in the neocortex and hippocampus express $Na_v1.1$. In support of a functional role of $Na_v1.1$ in PV interneurons, neocortical PV interneurons in an *Scn1a* mouse model of DS were unable to sustain high-frequency spike amplitudes following increasing current injections (Ogiwara et al., 2007). However, is it unknown whether altered *Scn1a* expression or function in PV interneurons is sufficient to cause epilepsy. Furthermore, a functional role for *Scn1a* in pyramidal cells has not been directly examined.

The purpose of this study is to directly compare the contribution of $Na_v1.1$ channels in inhibitory PV interneurons and excitatory pyramidal cells to seizure generation. To achieve this, we first generated mice that were heterozygous for a floxed *Scn1a* allele. This line was then crossed to transgenic mice that express Cre recombinase in order to preferentially inactivate the heterozygous floxed allele in either PV interneurons or pyramidal neurons of the neocortex and hippocampus. We found that the inactivation of one *Scn1a* allele in interneurons led to the generation of spontaneous generalized seizures and increased susceptibility to flurothyl- and hyperthermia-induced seizures; whereas seizure thresholds were unchanged following inactivation in pyramidal cells. Taken together, these findings provide evidence for a direct link between the function of $Na_v1.1$ channels in PV interneurons and *SCN1A*-derived epilepsy subtypes.

Materials and methods

Preparation of the targeting construct

The targeting construct was generated by cloning three PCR-generated fragments with homology to the *Scn1a* locus into the pFlexible vector (pLoxP-2FRT-PGKneo)(van der Weyden et al., 2005). Fragment 1 (3.8 kb), corresponding to the 5′ arm of homology, was amplified using the primer pair 1F/1R. Fragment 2 (750 bp), containing exon 1 and flanking non-coding sequences, was amplified using the primer pair 2F/2R. Fragment 3 (4.1 kb), the 3′ arm of homology, was amplified using the primer pair 3F/3R (Figure 1A). The assembled targeting construct was sequenced to confirm the absence of unwanted substitutions. Primer sequences are provided in Supplementary Table 1.

Targeting of mouse Scn1a

The targeting construct was linearized with *AvrII*, gel-purified, and electroporated into 129X1/SvJ-derived PAT-5 embryonic stem (ES) cells at the University of Michigan Transgenic Core. A total of 576 puromycin-resistant clones were selected and screened by PCR amplification for correct targeting of the 3′ arm using the primer F1 located in the puromycin gene, and R1 located in genomic sequence downstream of the 3′ arm. Positive clones were then screened for homologous recombination of the 5′ arm by PCR amplification using primer F4, located in the genomic sequence upstream of the 5′ arm, and the reverse primer R4, located in the puromycin gene. PCR reactions were performed with PCR SuperMix High Fidelity (Invitrogen, Carlsbad, CA) using the recommended conditions. Seven percent targeting efficiency was observed.

Southern blot hybridization

ES cell clones that amplified with both PCR screens were analyzed by Southern blot hybridization (Figure 1B). Ten micrograms of genomic DNA was digested overnight with *PacI/StuI* or *EcoR1*, and then separated by agarose gel electrophoresis. Gels were soaked in 0.25 M HCL for 10 min, 0.5 M NaOH/1.5 M NaCl for 20 min, and 1.5 M NaCl/0.5 M Tris (pH 7.5) for 20 min, and then transferred to Hybond-XL membranes (Amersham Biosciences) with 10 X SSC. Membranes were pre-hybridized at 65°C for 2 h in 7% SDS, 0.25 M Na_2HPO_4 (pH 7.2), and 1 mM EDTA. External probes with homology to the region upstream of the 5′ arm (5′E) and downstream of the 3′ arm (3′E) were PCR-amplified with the primer pairs 5′Fe/5′Re and 3′Fe/3′Re, respectively. Internal probes with homology to the 5′ (5′I) and 3′ (3′I) arms were amplified using the primer pairs 5′Fi/5′Ri and 3′Fi/3′Ri, respectively. Each probe was radiolabeled with [α-^{32}P] CTP using the Megaprime DNA Labeling System (Amersham Biosciences), purified using MicroSpin G-50 columns (Amersham Biosciences), and added to the prehybridization buffer for overnight incubation with the membrane. Membranes were washed twice with 2X SSC/0.1% SDS, once with 1X SSC/0.1% SDS, and once with 0.2X SSC/0.1% SDS at 65°C. Clones identified as correctly targeted were confirmed to have normal karyotypes by chromosome analysis. Southern blot analysis of genomic DNA from tail biopsies of five-week-old mice was performed as described for the ES cell clones.

Generation of mice with a heterozygous floxed allele (Scn1a$^{Flox/+}$)

Two correctly targeted clones were injected into blastocysts obtained from mating C57BL/6NCrl female mice with (C57BL/6J X DBA/2J) F1 male mice. Male chimeras with a high percentage of agouti coat color were bred to B6;SJL-Tg(ACTFLPe)9205Dym/J females expressing *FLP1* recombinase to test for germline transmission of the floxed allele and to delete the puromycin cassette. *Scn1a*$^{Flox/+}$; B6;SJL-Tg(ACTFLPe)9205Dym/J male offspring were then bred to C57BL/6J females, and *Scn1a*$^{Flox/+}$ N1 males that lacked the FLPe transgene were identified. Using the primer pair X1-F2/X1-R2, the floxed *Scn1a* allele and the WT allele generated 845-bp and 750-bp PCR products, respectively. *Scn1a*$^{Flox/+}$ male mice were then backcrossed three times onto the C57BL/6J background to generate the N4 generation that was used for all subsequent experiments. Mice were maintained at 22°C on a 12-h light/dark cycle, and food and water were available *ad libitum.* All experiments were performed in accordance with the Institutional Animal Care and Use Committee of Emory University.

Protein extraction

Whole brains from 22-day-old (P22) *Scn1a*$^{Flox/+}$ mice and wildtype (WT) littermates were homogenized in 10 ml of 50 mM Tris (pH = 7.5), 10 mM EGTA, and one complete EDTA-free protein inhibitor tablet (Roche). The lysates were centrifuged at 3,500 rpm for 10 min at 4°C. The supernatant was removed and centrifuged at 38,000 rpm for 30 min at 4°C. The pellet, containing the membrane-bound proteins, was suspended in the same buffer used for homogenization, and protein concentration was determined.

Western blot analysis

Western blot analysis was performed on whole brains from P22 mice as previously described (Martin et al., 2010). Briefly, 25 μg of extracted protein was separated on a 7.5% polyacrylamide Tris-HCL gel and transferred to a PVDF membrane. Membranes were blotted with anti-$Na_V1.1$ (Millipore, 1:200) and anti-α-tubulin (Abcam, 1:10,000) antibodies. The secondary antibodies, anti-rabbit IgG (GE, 1:5,000) and anti-mouse IgG (Jackson, 1:5,000), diluted in TBST, were used to identify $Na_V1.1$ and α-tubulin, respectively. The membranes were developed with a chemiluminescent agent (HyGLO Quick Spray, Denville Scientific).

Immunohistochemistry

Immunohistochemistry was performed on three wild-type C57BL/6J mice (P22) to examine the expression of $Na_V1.1$ in PV interneurons and calmodulin-dependent protein kinase (*CaMK2α*)-positive pyramidal neurons. Mice expressing yellow fluorescence protein (YFP) under the Thy1 promoter (Thy1-YFP) (Jackson Laboratories, Bar Harbor, ME) were also used to analyze the expression of $Na_V1.1$ in excitatory cells. Mice were deeply anesthetized with isoflurane and transcardially perfused. Brains were post-fixed in paraformaldehyde (4%), cryopreserved in 30% sucrose, and 45 μm sections were cut on a cryostat (Leica, Germany). Coronal sections, 400 μm apart, from bregma -0.46 mm to -3.38 mm, were examined. Free-floating sections were washed in TBS/Triton X and blocked in 2% avidin and then 2% biotin. Sections were then incubated with polyclonal rabbit anti-*Scn1a* (1:50,

Millipore) and either monoclonal mouse anti-*CaMK2α* (1/200, Millipore) or mouse monoclonal anti-parvalbumin (1:1000, Swant). After washing, sections were incubated in secondary antibodies, biotinylated anti-rabbit IgG (1:300, Vector Laboratories) and Alexa Fluor 555 anti-mouse IgG (1:1000, Invitrogen), followed by washing and incubation in fluorescein avidin D (1:300, Vector Laboratories). Negative controls included sections that were not incubated with primary antibody, and sections from P2-3 neonatal mouse pups that do not express detectable levels of $Na_v1.1$. Sections were mounted and visualized using confocal microscopy (Carl Zeiss LSM 510 META). Cells were counted using lmaris software (Bitplane Scientific solutions) on images captured under 40X and 10X magnification. Results from three different animals were combined for the analysis of each sodium channel/cell-type combination.

Generation of heterozygous Scn1a-deleted mice

We used primers and PCR conditions provided by The Jackson Laboratory (Bar Harbor, ME) to screen for the presence of each *Cre* transgene. Three different *Cre* transgenic lines were used to excise the floxed *Scn1a* allele: *ZP3-Cre*, *Ppp1r2-Cre*, and *EMX1*$^{tm(cre)Krj}$/J - *Cre*. All *Cre* transgenic lines were maintained on a C57BL/6J background. A 215-bp PCR product identified mice that were positive for the deleted (inactivated) allele. The *ZP3-Cre* line, which produces global deletion, was used to demonstrate that the floxed allele could be effectively inactivated. Male *Scn1a*$^{Flox/+}$ mice were crossed to female C57BL/6-Tg(Zp3-cre)93Knw/J (*ZP3-Cre*) mice (Jackson Laboratory, Bar Harbor, ME) expressing Cre recombinase in the female germline. Female offspring carrying the floxed allele and the *ZP3-Cre* transgene were then crossed to wild-type C57BL/6J males, resulting in offspring that were heterozygous for inactivation of the floxed allele. The *EMX1*$^{tm(cre)Krj}$/J (*EMX-Cre*, Jackson Laboratory, Bar Harbor, ME) and *Ppp1r2-Cre* (Belforte et al., 2010) lines were used to determine the effect of preferentially inactivating *Scn1a* from excitatory pyramidal neurons and parvalbumin (PV) inhibitory interneurons in the neocortex and hippocampus, respectively. Specifically, the *EMX-Cre* line expresses *Cre* recombinase in glutamatergic neurons in the telencephalon, which includes the neocortex, hippocampus, and amygdala (Gorski et al., 2002), whereas the *Ppp1r2-Cre* line predominately expresses *Cre* recombinase in PV inhibitory interneurons in the neocortex and hippocampus (Belforte et al., 2010). Female *Scn1a*$^{Flox/+}$ mice (N4 with respect to C57BL/6J) were crossed to either male *EMX-* or *Ppp1r2-Cre* mice. Mice that were heterozygous for the floxed allele and carried the *Cre* transgene (*Scn1a*$^{Flox/+}$/*Cre*$^{+/-}$) were our experimental mutants. Controls were *Scn1a*$^{Flox/+}$ progeny that lacked the *Cre* transgene (*Scn1a*$^{Flox/+}$/*Cre*$^{-/-}$), progeny that lacked the targeted allele, but carried the *Cre* transgene (*Scn1a*$^{+/+}$/*Cre*$^{+/-}$), and progeny that lacked the targeted allele and the *Cre* transgene (*Scn1a*$^{+/+}$).

Flurothyl seizure induction

Flurothyl seizure induction was performed as previously described (Martin et al., 2010). Briefly, mice (2–3 months old) were placed in a clear acrylic glass chamber and flurothyl (2,2,2-trifluroethylether, Sigma-Aldrich) was introduced at a rate of 20 μl/min. Latencies to the first myoclonic jerk (MJ) and to the generalized tonic-clonic seizure (GTCS) were recorded.

Febrile seizure induction

Thresholds to hyperthermia-induced seizures (a measure of febrile seizure susceptibility) were determined as previously described (Oakley et al., 2009). Briefly, each mouse (P22), placed in an acrylic glass cylinder, was fitted with a rectal temperature probe that was connected to a heating lamp via a temperature controller (TCAT 2DF, Physitemp). The selection of 22-day-old mice for this experiment was based on previous observations that *Scn1a* mutant mice are highly susceptible to hyperthermia-induced seizures at this age (Oakley et al., 2009, Dutton et al., in preparation). Each mouse was held at 37.5°C for 10 minutes to acclimatize it to the chamber. Body temperature was then elevated by 0.5°C every 2 minutes until either a seizure occurred or a maximum temperature of 42.5°C was reached. Seizure behavior was graded using a modified Racine Scale: 1, staring; 2, head nodding; 3, unilateral forelimb clonus; 4, bilateral forelimb clonus; 5, rearing and falling; 6, generalized seizure. In separate cohorts of mice (P22), seizure induction was coupled with real-time digital video-electroencephalographic (EEG) recordings.

EEG surgery and real-time video/EEG acquisition during febrile seizure induction

Six P22 $Scn1a^{Flox/+}/Ppp1r2\text{-}Cre^{+/-}$ mice and four $Scn1^{Flox/+}$ control mice were anesthetized with isoflurane and surgically implanted with two pairs of stainless steel sterile screw electrodes (0.10 inch in diameter; Pinnacle Technology, Inc.). The first pair of electrodes was placed posterior to bregma in the right hemisphere (EEG_1 and EEG_2), and the second pair of electrodes was placed at the corresponding positions in the left hemisphere (EEG_3 and EEG_4). Following electrode placement, fine wires were wrapped tightly around each screw and dental acrylic was applied. Following 2 hours of recovery from surgery, each mouse was subjected to the febrile seizure induction paradigm and real-time video and EEG signals were collected, processed, and digitized at a sampling rate of 200 Hz by the Stellate Harmonie amplifier and software (Natus Medical, Inc.).

EEG surgery and real-time video/EEG/EMG acquisition from freely moving adult mice (P60–90)

Under isoflurane anesthesia, six $Scn1a^{Flox/+}/Ppp1r2\text{-}Cre^{+/-}$ mice and seven $Scn1^{Flox/+}$ control mice were implanted subdurally with four stainless steel sterile screw electrodes (Vintage Machine Supplies, Medina, OH) for EEG acquisition at the following coordinates: Right hemisphere - EEG_1; 2 mm anterior-posterior (AP) and 1.2 mm lateral to the midline (LM), EEG_2; 1.5 mm AP and 1.2 mm LM, Left hemisphere - EEG_3; 0.5 mm AP and 2.2 LM, EEG_4; 3.5 mm AP and 2.2 mm LM, and fine-wire electrodes were inserted into the neck muscle for electromyography (EMG) activity as previously described (Martin et al., 2010; Papale et al., 2009). After a minimum of five days recovery from surgery, each mouse was individually placed into an acrylic glass box (15 × 15 × 15 cm) and attached to the EEG system via a small counterbalance (Dragonfly Research). Following 24 hours of acclimatization, each animal was subjected to 96 hours of continuous digital video/EEG/EMG recordings that were collected, processed, and digitized at a sampling rate of 200 Hz by Stellate Harmonie amplifier and software (Natus Medical, Inc.).

EEG/EMG scoring and data analysis

EEG signals were analyzed using a high-pass filter of 0.5 Hz and a low-pass filter of 35 Hz. EMG signals were analyzed using a high-pass filter of 10 Hz and a low-pass filter of 70 Hz. The calibration mark during EEG analysis was 30 μV/mm and 1 second. EEG recordings were manually scored using three different EEG/EMG montages. For the first EEG/EMG montage, the muscle electrode served as the reference for each of the four cortical electrodes (e.g. EEG_1-EMG_1, Figure 9). To eliminate possible muscle artifacts, the second EEG/EEG montage was generated by referencing the cortical electrodes on the right and left hemispheres to each other (e.g. EEG_1-EEG_2, Supplementary Figure 2). The third montage was used for the analysis of the EEG data from P22 mice during FS induction. For this montage, the same cortical electrode (EEG_4) served as the reference for the other three cortical electrodes (e.g. EEG_1- EEG_4, Figure 8) since muscle electrodes were not implanted. Epileptiform activity was characterized by the onset of sharp waves that increased in frequency and achieved amplitudes that were at least two times the background with detection in all cortical EEG channels and attenuation of the background rhythm. Simultaneous video recordings enabled the behavior of each animal to be observed during the seizure (Supplementary Videos 1 and 2).

Statistical analysis

A one-way analysis of variance (ANOVA) followed by Tukey's post-hoc analysis was used to identify statistically significant differences in thresholds to flurothyl-induced seizures between mice with restricted deletion of *Scn1a* and control littermates. Data are represented as mean ± standard error of the mean (SEM). Statistical significance was defined as $p < 0.05$.

Results

Generation of the floxed Scn1a allele

We generated an *Scn1a* conditional knock-out mouse model in which exon 1 of the mouse *Scn1a* gene is flanked by LoxP sites (Figure 1A). Five hundred and seventy six neomycin-resistant ES cell clones were screened for correct targeting by PCR amplification of the 5′ and 3′ regions of homology. Clones that were positive in both PCR assays were also examined by Southern blot analysis. Two correctly targeted ES cell clones were injected into blastocysts to generate chimeric mice that were bred to generate the conditional knock-out mice. The presence of the targeted allele in the resulting lines of mice was confirmed by Southern blot analysis with 5′ and 3′ internal and external probes (Figure 1B).

The floxed allele does not alter $Na_v1.1$ levels

Western blot analysis was performed on protein extracts from whole brains of $Scn1a^{Flox/+}$ mice and WT littermates to determine whether the presence of the floxed allele affected $Na_v1.1$ protein levels. Figures 2A and 2B show comparable levels of $Na_v1.1$ for both genotypes, demonstrating that the presence of the floxed allele did not alter expression.

The floxed allele does not alter seizure thresholds

Scn1a$^{Flox/+}$ mice (n = 8) and their WT littermates (n = 9) were evaluated for susceptibility to flurothyl-induced seizures. No differences were observed in latencies to the MJ (WT: 309 ± 12 sec, *Scn1a*$^{Flox/+}$: 307 ± 17 sec; p>0.05) or GTCS (WT: 418 ± 17 sec, *Scn1a*$^{Flox/+}$: 427 ± 32 sec; p>0.05) between genotypes, indicating that the presence of the floxed allele did not alter seizure thresholds.

Scn1a$^{Flox/+}$/Zp3-Cre$^{+/-}$ mutants exhibit spontaneous seizures and shortened life spans

Twenty-three *Scn1a*$^{Flox/+}$*/Zp3-Cre*$^{+/-}$ mice were continuously video-recorded from 21 to 28 days of age (total of 168 hours each) and the frequency of spontaneous seizures was determined using the Seizure Scan system (CleverSys, Inc.). The Seizure Scan system provides continuous video recording of freely moving mice. The recorded video files were analyzed using a seizure detection algorithm that is capable of identifying seizure-like behaviors. The detected seizure-like behaviors were then manually examined to confirm the occurrence of a behavioral seizure. Spontaneous seizures were observed in 12 *Scn1a*$^{Flox/+}$*/ Zp3-Cre*$^{+/-}$ mice (52.3%) and occurred at an average frequency of three per day. Seizures lasted an average of 35 seconds and were characterized by jumping, repetitive jerking of all four limbs, head nodding, and clonus of the forelimbs and tail. Some behavioral seizures ended with hindlimb extension, typical of severe seizures in the mouse. The average life span of the *Scn1a*$^{Flox/+}$*/Zp3-Cre*$^{+/-}$ mutants was 33 days. The reduced lifespan and spontaneous seizure frequency of the *Scn1a*$^{Flox/+}$*/Zp3-Cre*$^{+/-}$ mutants were similar to heterozygous *Scn1a* knockout mice (Yu et al., 2006), indicating the effective inactivation of the floxed *Scn1a* allele. Seizures were not detected in control littermates that lacked the *Cre* transgene.

$Na_v1.1$ is expressed in PV-interneurons and excitatory cells of the mouse hippocampus and neocortex

Immunohistochemistry was performed on brain sections from P22 mice to determine the relative expression of $Na_v1.1$ in PV-expressing interneurons and *CaMK2α* and Thy1-YFP expressing excitatory neurons. We found that 69% (234/338) of $Na_v1.1$ immunoreactive cells in the hippocampus were PV-immunoreactive, and most (91%, 234/256) of PV-immunoreactive interneurons in the hippocampus were also $Na_v1.1$ immunoreactive (Figure 3A). However, the extent of co-localization varied between hippocampal regions (Supplementary Figure 1, 10X images). On average, 75% (196/263) of $Na_v1.1$-positive neurons in the CA1, CA3, and the DG regions of the hippocampus were PV-positive, and 91% (196/216) of PV-positive neurons in these regions were also $Na_v1.1$-positive. In the dentate hilus and the stratum radiatum/stratum lacunosum-moleculare (SR/SLM) 47% (7/15) and 52% (31/60) of $Na_v1.1$-immunoreactive cells were PV positive, respectively, while 78% (7/9) of PV-positive cells in the dentate hilus and 97% (38/39) in the SR/SLM co-localized with $Na_v1.1$ immunoreactivity. Thirteen percent (24/179) and 1% (1/74) of $Na_v1.1$-positive cells were *CaMK2α*-immunoreactive and Thy1-YFP-positive in the hippocampus, respectively (Figure 3B and 3C).

Extensive overlap of $Na_v1.1$ and PV immunoreactivity was also detected in the neocortex. We observed that 69% (36/52) of $Na_v1.1$-immunoreactive cells were PV-positive, and 78%

(47/60) of PV-positive neurons were immunoreactive for $Na_v1.1$ in layers 2–6 (Figure 4A). In contrast, only 5% (3/62) of $Na_v1.1$-immunoreactive cells were positive for *CaMK2α* in layers 2–6 of the neocortex (Figure 4B). No co-localization was observed between $Na_v1.1$ and Thy1-YFP-positive excitatory cells in layers 2/3 and 5 of the cortex (0/84) (Figure 4C). Most Thy1-YFP cells were *CaMK2α*-positive in layers 2/3 and 5 of the hippocampus (94%, 50/53) whereas a relatively small percentage of *CaMK2α*-positive layer 2/3 and 5 cortical neurons were Thy1-YFP positive (9%, 50/435).

Preferential inactivation of Scn1a in corticolimbic PV interneurons reduces thresholds to flurothyl-induced seizures

Having observed $Na_v1.1$ expression in PV-positive neurons and excitatory cells of the hippocampus and neocortex, we next examined the effect on seizure thresholds of preferentially reducing the expression of *Scn1a* in either PV interneurons (*Scn1a*$^{Flox/+}$/*Ppp1r2-Cre*$^{+/-}$ mice) or excitatory pyramidal cells (*Scn1a*$^{Flox/+}$*/EMX-Cre*$^{+/-}$ mice) primarily in the neocortex and hippocampus. Deletion of the heterozygous floxed *Scn1a* allele by both *Cre* transgenes was confirmed by the presence of the predicted 215-bp fragment following PCR amplification of tissue from neocortex and hippocampus of *Scn1a*$^{Flox/+}$*/Ppp1r2-Cre*$^{+/-}$ and *Scn1a*$^{Flox/+}$*/EMX-Cre*$^{+/-}$ mice (Figure 5). Mice with preferential deletion of *Scn1a* from both lines exhibited normal lifespans.

Thresholds to flurothyl-induced seizures following inactivation of one *Scn1a* allele in interneurons were determined by comparing seizure latencies between *Scn1a*$^{Flox/+}$*/Ppp1r2-Cre*$^{+/-}$ mice and control littermates (*Scn1a*$^{+/+}$, *Scn1a*$^{+/+}$*/Ppp1r2-Cre*$^{+/-}$, and *Scn1a*$^{Flox/+}$). Twelve mice of each genotype were evaluated. Average latencies to the MJ were comparable between all genotypes (*Scn1a*$^{+/+}$: 286 ± 9 s, *Scn1a*$^{+/+}$*/Ppp1r2-Cre*$^{+/-}$: 285 ± 10 s, *Scn1a*$^{Flox/+}$: 285 ± 6 s, *Scn1a*$^{Flox/+}$*/Ppp1r2-Cre*$^{+/-}$: 282 ± 13 s; $p = 0.1$; Figure 6A). In contrast, the *Scn1a*$^{Flox/+}$*/Ppp1r2-Cre*$^{+/-}$mutants exhibited a 15–19% reduction in latency to the GTCS compared with the other genotypes (*Scn1a*$^{+/+}$: 374 ± 18 s, *Scn1a*$^{+/+}$*/ Ppp1r2-Cre*$^{+/-}$: 353 ± 18 s, *Scn1a*$^{Flox/+}$: 354 ± 15 s, *Scn1a*$^{Flox/+}$*/Ppp1r2-Cre*$^{+/-}$: 301 ± 10 s, $p = 0.0001$, Figure 6A).

Seizure thresholds were similarly evaluated following the inactivation of the floxed *Scn1a* allele in excitatory neurons. When the *Scn1a*$^{Flox/+}$*/EMX-Cre*$^{+/-}$ mice (n = 16) were compared to the control littermates (*Scn1a*$^{+/+}$ (n = 16), *Scn1a*$^{+/+}$*/EMX-Cre*$^{+/-}$ (n = 19), *Scn1a*$^{Flox/+}$ (n = 16)), similar average latencies were observed for the MJ (*Scn1a*$^{+/+}$: 287 ± 18 s, *Scn1a*$^{+/+}$*/EMX-Cre*$^{+/-}$: 333 ± 15 s, *Scn1a*$^{Flox/+}$: 322 ± 17 s, *Scn1a*$^{Flox/+}$*/EMX-Cre*$^{+/-}$: 321 ± 8 s, $p = 0.2$) and GTCS (*Scn1a*$^{+/+}$: 459 ± 26 s, *Scn1a*$^{+/+}$*/EMX-Cre*$^{+/-}$: 435 ± 14 s, *Scn1a*$^{Flox/+}$: 416 ± 18 s, *Scn1a*$^{Flox/+}$*/EMX-Cre*$^{+/-}$: 433 ± 16 s, $p = 0.5$) (Figure 6B).

Preferential inactivation of Scn1a in corticolimbic PV interneurons reduces latency to hyperthermia-induced seizures

Given the frequent occurrence of febrile seizures in patients with *SCN1A* mutations, we also determined whether thresholds for hyperthermia-induced seizures were altered following preferential inactivation of the floxed *Scn1a* alelle in PV interneurons. The body temperature of *Scn1a*$^{Flox/+}$*/Ppp1r2-Cre*$^{+/-}$ and *Scn1a*$^{Flox/+}$ mice (P22–23) was increased by 0.5°C every

two minutes, until either a seizure was observed or a maximum temperature of 42.5°C was achieved. All mice were video recorded, and a subset was monitored with simultaneous video-EEG analysis. The latency, severity, and temperature at which the seizure occurred were determined for each mouse. No seizures were observed in *Scn1a*$^{Flox/+}$ controls (0/12); in contrast, we detected seizures in 75% (9/12) of the *Scn1a*$^{Flox/+}$*/Ppp1r2-Cre*$^{+/-}$ mutants (Figure 7). The average latency to seizure onset was 701 ± 48 s and occurred at an average temperature of 40.7 ± 0.2°C. Seizures achieved an average Racine score of 2.4 ± 0.1 and were characterized by sudden behavioral arrest, followed by head nodding and/or unilateral forelimb clonus. Behavioral seizures had an average duration of 11 ± 3 s and were associated with spike discharges on the EEG that were at least two times higher than the background (Figure 8A). Supplementary Video 1 provides an example of the behavior exhibited during a hyperthermia-induced seizure.

Thresholds to hyperthermia-induced seizures were similarly examined in *Scn1a*$^{Flox/+}$*/EMX-Cre*$^{+/-}$ mice and *Scn1a*$^{Flox/+}$ control littermates. Twelve mice of each genotype were evaluated. Neither genotype exhibited hyperthermia-induced seizures, based on behavioral observations and simultaneous video-EEG analysis (Figure 7, Figure 8B).

Preferential inactivation of Scn1a in corticolimbic PV interneurons leads to spontaneous seizures

Continuous EEG recordings were obtained for 96 hours from each of six *Scn1a*$^{Flox/+}$*/Ppp1r2-Cre*$^{+/-}$ and seven *Scn1a*$^{Flox/+}$ mice. Normal EEG patterns consisting of waveforms that increased and decreased in amplitude and frequency and were associated with EMG signals that displayed frequent alterations in muscular tone were observed in all animals (Figure 9A). Interestingly, two episodes of spontaneous seizures were observed in one *Scn1a*$^{Flox/+}$*/Ppp1r2-Cre*$^{+/-}$ mouse prior to the surgical procedure. The seizures, which lasted about seven seconds, involved vocalization accompanied by forelimb and tail clonus. Although we did not detect any spontaneous seizures during the EEG recording of this mouse, rhythmic high amplitude single spike discharges that were often accompanied by sudden jerking movements of the neck and body were observed (Figure 9B, Supplementary Figure 2). In another *Scn1a*$^{Flox/+}$*/Ppp1r2-Cre*$^{+/-}$ mouse, three spontaneous seizures with an average duration of 22 ± 2 seconds were detected. These seizures, which lacked obvious behavioral components, were characterized by high amplitude spike discharges that were first observed in the temporal region of the right hemisphere (EEG_2 channel, Figure 9C) with subsequent detection in all EEG channels and abrupt termination and return to normal waveform activity (Figure 9C, Supplementary Video 2). The remaining Scn1a$^{Flox/+}$/Ppp1r2-Cre$^{+/-}$ mice and the Scn1a$^{Flox/+}$ control mice did not show any EEG abnormalities.

Discussion

In the current study we generated an *Scn1a* conditional knockout line that, following global deletion of *Scn1a*, recapitulated the reduced lifespan and spontaneous seizures observed in the *Scn1a* knock-out mouse (a model of DS) and the R1648H GEFS+ mouse model (Yu et al., 2006; Martin et al., 2010). The conditional knockout line was then used to determine the effect of preferentially inactivating $Na_v1.1$ from PV interneurons and excitatory cells. We

found that preferential inactivation of one *Scn1a* allele in PV interneurons was sufficient to increase susceptibility to flurothyl- and hyperthermia-induced seizures and lead to spontaneous seizure generation. In contrast, similar inactivation of *Scn1a* from excitatory cells did not significantly alter seizure thresholds.

In agreement with our findings from the analysis of seizure thresholds, *Scn1a* expression was detected in a large percentage of PV-interneurons in the hippocampus and neocortex, whereas only a small percentage of $Na_v1.1$-positive cells expressed *CaMK2α*. $Na_v1.1$ expression in pyramidal cells has been previously reported. Using immunohistochemistry, Ogiwara et al. (2007) observed minor staining of $Na_v1.1$ in the pyramidal cell layer of the hippocampus. In contrast, Gong and colleagues (1999) reported intense immunoreactivity for $Na_v1.1$ in the cell bodies and dendrites of neurons located within the stratum pyramidale, CA1 – CA3 and the molecular layer of the dentate gyrus. In these previous studies, pyramidal cell identity was based on cell morphology and location and $Na_v1.1$ expression was determined from the intensity of the fluorescent signal. In the current study, we determined the percentage of cells that were positive for both $Na_v1.1$ and the pyramidal cell markers, *CaMK2α* and *Thy1*. The results from our study are consistent with broad expression of *Scn1a* in PV interneurons and much more limited expression in pyramidal cells in the hippocampus and cortex.

It is noteworthy that the phenotype of the $Scn1a^{Flox/+}/Ppp1r2\text{-}Cre^{+/-}$ mutants was less severe than heterozygous *Scn1a* knockout mice (Yu et al., 2006) and $Scn1a^{Flox/+}/Zp3\text{-}Cre^{+/-}$ mice. Several factors are likely to account for this observation. Firstly, inactivation of the floxed allele was restricted to the forebrain in $Scn1a^{Flox/+}/Ppp1r2\text{-}Cre^{+/-}$ mutants whereas global deletion would have occurred on the other lines. Secondly, Belforte et al. (2010) reported that the $Ppp1r2\text{-}Cre^{+/-}$ line targets approximately 75% of PV-expressing interneurons in the hippocampus and neocortex. Therefore, incomplete targeting of forebrain PV interneurons would be predicted in $Scn1a^{Flox/+}/Ppp1r2\text{-}Cre^{+/-}$ mutants. Thirdly, we observed that approximately 50% of $Na_v1.1$-positive neurons in the hilus and stratum radiatum do not have PV immunoreactivity, suggesting that *Scn1a* may play a functional role in additional interneuron subtypes. Although the $Ppp1r2\text{-}Cre^{+/-}$ line primarily targets PV interneurons, Belforte et al (2010) also observed *Cre*-mediated deletion in 30% of Reelin-positive interneurons, 15% of neuropeptide Y-expressing interneurons, and some somatostatin-expressing interneurons (Belforte et al., 2010). However, the expression of *Scn1a* in these and other interneuron subtypes has not been well characterized.

PV interneurons have previously been demonstrated to play a role in other epilepsy models as well as in human epilepsy. Schwaller et al. (2004) reported that PV knockout mice display increased susceptibility to pentylenetetrazole-induced seizures compared with WT littermates. Loss of PV interneurons has also been seen following chemically (Buckmaster & Dudek, 1997) and electrically induced seizures (Gorter et al., 2001). In addition, reduced PV immunoreactivity has been found in several rodent models of epilepsy (Magloczky & Freund, 1995; Scotti et al., 1997; Sloviter et al., 2003) and following recurrent hyperthermia-induced seizures (Kwak et al., 2008). Clinically, patients with intractable temporal lobe epilepsy also show reduced PV expression in resected neocortex (Marco et al., 1996; de Lanerolle et al., 1989). However, it is unclear whether these observed reductions in

PV immunoreactivity are due to a decrease in the level of the PV protein itself or indicative of neuronal damage or degeneration.

In addition to epilepsy, altered PV interneuron function has been implicated in the pathophysiology of several neuropsychiatric and neurodevelopmental disorders. Epilepsy and schizophrenia have been shown to be co-morbid (Chang et al., 2011), and post mortem brains of schizophrenia patients show decreased density of PV interneurons (Mirnics et al., 2000; Vawter et al., 2002; Woo et al., 2004). Reduced messenger RNA levels for parvalbumin and decreased density of PV interneurons have also been observed in the hippocampus of post mortem brains of patients with bipolar disorder (Knable et al., 2004). PV interneurons are also important for the generation of gamma (γ) oscillations that occur in the 30–100 Hz frequency range. Altered γ oscillations have been identified in epileptic patients (Kobayashi et al., 2004; Wendling et al., 2002) and rodent models of epilepsy (Ma & Leung, 2002; Medvedev, 2001). Gamma oscillations are also required for working memory function, suggesting that altered PV interneuron function may underlie the impairments in working memory that are observed in disorders such as schizophrenia (Haenschel et al., 2009). In contrast to schizophrenia and bipolar disorder, an increase in the number of PV-immunoreactive interneurons was observed in the CA1 and CA3 regions of the hippocampus in a small study of post mortem brains from five individuals with autism (Lawrence et al., 2010). Interestingly, approximately twenty percent of individuals with autism also develop epilepsy and a *de novo* missense *SCN1A* mutation was recently identified in a patient with autism spectrum disorder (O'Roak et al., 2011). Some individuals with Dravet syndrome also display autistic features (Bolton et al., 2011; Genton et al., 2011; Li et al., 2011). Given the importance of $Na_v1.1$ to PV interneuron function, *SCN1A* should be considered a candidate gene for disorders that are associated with altered PV interneuron function and, in particular, those that are co-morbid with epilepsy.

Finally, it should be noted that while pyramidal cell-specific expression of *Scn1a* does not appear to play a major role in seizure generation, we cannot exclude the possibility that it may be functionally important and could potentially contribute to other neurological disorders.

Conclusions

In summary, we found that preferential inactivation of one *Scn1a* allele in PV interneurons of the neocortex and hippocampus results in reduced seizure thresholds, whereas similar inactivation of *Scn1a* from excitatory neurons does not significantly affect seizure thresholds. This work represents the first direct demonstration of a causal relationship between loss of $Na_v1.1$ in a particular neuronal subtype and seizure susceptibility. The identification of critical neuronal subtypes that contribute to *SCN1A*-derived disorders could pave the way for the development of novel cell-type specific treatment strategies.

Supplementary Material

Refer to Web version on PubMed Central for supplementary material.

Acknowledgments

We would like to thank the laboratory of Dr. William Catterall for assistance with the hyperthermia seizure induction paradigm and guidance with immunohistochemistry. We are grateful to Cheryl Strauss for editorial assistance. This study was supported by grants from the NIH (R01 NS072221 to AE, and 1F31 NS065694 to SBD) and by a predoctoral fellowship from the Epilepsy Foundation (SBD). This research was also supported in part by the NINDS core facilities grant P30N5055077 to the Emory University Microscopy Core.

References

Barela AJ, Waddy SP, Lickfett JG, Hunter J, Anido A, Helmers SL, et al. An epilepsy mutation in the sodium channel SCN1A that decreases channel excitability. J Neurosci. 2006; 26:2714–23. [PubMed: 16525050]

Belforte JE, Zsiros V, Sklar ER, Jiang Z, Yu G, Li Y, et al. Postnatal NMDA receptor ablation in corticolimbic interneurons confers schizophrenia-like phenotypes. Nat Neurosci. 2010; 13:76–83. [PubMed: 19915563]

Bolton PF, Carcani-Rathwell I, Hutton J, Goode S, Howlin P, Rutter M. Epilepsy in autism: features and correlates. Br J Psychiatry. 2011; 198:289–94. [PubMed: 21972278]

Buckmaster PS, Dudek FE. Neuron loss, granule cell axon reorganization, and functional changes in the dentate gyrus of epileptic kainate-treated rats. J Comp Neurol. 1997; 385:385–404. [PubMed: 9300766]

Catterall WA, Kalume F, Oakley JC. NaV1.1 channels and epilepsy [Review]. J Physiol. 2010; 588:1849–59. [PubMed: 20194124]

Chang YT, Chen PC, Tsai IJ, Sung FC, Chin ZN, Kuo HT, et al. Bidirectional relation between schizophrenia and epilepsy: A population-based retrospective cohort study. Epilepsia. 2011; 52:2036–42. [PubMed: 21929680]

Claes L, Del-Favero J, Ceulemans B, Lagae L, Van Broeckhoven C, De Jonghe P. De novo mutations in the sodium-channel gene SCN1A cause severe myoclonic epilepsy of infancy. Am J Hum Genet. 2001; 68:1327–32. [PubMed: 11359211]

de Lanerolle NC, Kim JH, Robbins RJ, Spencer DD. Hippocampal interneuron loss and plasticity in human temporal lobe epilepsy. Brain Res. 1989; 495:387–95. [PubMed: 2569920]

Escayg A, Goldin AL. Sodium channel *Scn1a* and epilepsy: mutations and mechanisms [Review]. Epilepsia. 2010; 51:1650–8. [PubMed: 20831750]

Escayg A, MacDonald BT, Meisler MH, Baulac S, Huberfeld G, An-Gourfinkel I, et al. Mutations of SCN1A, encoding a neuronal sodium channel, in two families with GEFS+2. Nat Genet. 2000; 24:343–5. [PubMed: 10742094]

Genton P, Velizarova R, Dravet C. Dravet syndrome: the long-term outcome. Epilepsia. 2011; 52 (Suppl 2):44–9. [PubMed: 21463279]

Gong B, Rhodes KJ, Bekele-Arcuri Z, Trimmer JS. Type I and type II Na(+) channel alpha-subunit polypeptides exhibit distinct spatial and temporal patterning, and association with auxiliary subunits in rat brain. J Comp Neurol. 1999; 412:342–52. [PubMed: 10441760]

Gorski JA, Talley T, Qiu M, Puelles L, Rubenstein JL, Jones KR. Cortical excitatory neurons and glia, but not GABAergic neurons, are produced in the Emx1-expressing lineage. J Neurosci. 2002; 22:6309–14. [PubMed: 12151506]

Gorter JA, van Vliet EA, Aronica E, Lopes da Silva FH. Progression of spontaneous seizures after status epilepticus is associated with mossy fibre sprouting and extensive bilateral loss of hilar parvalbumin and somatostatin-immunoreactive neurons. Eur J Neurosci. 2001; 13:657–69. [PubMed: 11207801]

Grant AC, Vazquez B. A case of extended spectrum GEFS+ Epilepsia. 2005; 46 (Suppl 10):39–40. [PubMed: 16359470]

Haenschel C, Bittner RA, Waltz J, Haertling F, Wibral M, Singer W, et al. Cortical oscillatory activity is critical for working memory as revealed by deficits in early-onset schizophrenia. J Neurosci. 2009; 29:9481–9. [PubMed: 19641111]

Knable MB, Barci BM, Webster MJ, Meador-Woodruff J, Torrey EF. Molecular abnormalities of the hippocampus in severe psychiatric illness: postmortem findings from the Stanley Neuropathology Consortium. Mol Psychiatry. 2004; 9:609–20. 544. [PubMed: 14708030]

Kobayashi K, Oka M, Akiyama T, Inoue T, Abiru K, Ogino T, et al. Very fast rhythmic activity on scalp EEG associated with epileptic spasms. Epilepsia. 2004; 45:488–96. [PubMed: 15101830]

Kwak SE, Kim JE, Kim SC, Kwon OS, Choi SY, Kang TC. Hyperthermic seizure induces persistent alteration in excitability of the dentate gyrus in immature rats. Brain Res. 2008; 1216:1–15. [PubMed: 18495095]

Lawrence YA, Kemper TL, Bauman ML, Blatt GJ. Parvalbumin-, calbindin-, and calretinin-immunoreactive hippocampal interneuron density in autism. Acta Neurol Scand. 2010; 121:99–108. [PubMed: 19719810]

Li BM, Liu XR, Yi YH, Deng YH, Su T, Zou X, et al. Autism in Dravet syndrome: prevalence, features, and relationship to the clinical characteristics of epilepsy and mental retardation. Epilepsy Behav. 2011; 21:291–5. [PubMed: 21620773]

Ma J, Leung LS. Metabotropic glutamate receptors in the hippocampus and nucleus accumbens are involved in generating seizure-induced hippocampal gamma waves and behavioral hyperactivity. Behav Brain Res. 2002; 133:45–56. [PubMed: 12048173]

Magloczky Z, Freund TF. Delayed cell death in the contralateral hippocampus following kainate injection into the CA3 subfield. Neuroscience. 1995; 66:847–60. [PubMed: 7651613]

Mahoney K, Moore SJ, Buckley D, Alam M, Parfrey P, Penney S, et al. Variable neurologic phenotype in a GEFS+ family with a novel mutation in SCN1A. Seizure. 2009; 18:492–7. [PubMed: 19464195]

Marco P, Sola RG, Pulido P, Alijarde MT, Sanchez A, Ramon y Cajal S, et al. Inhibitory neurons in the human epileptogenic temporal neocortex. An immunocytochemical study. Brain. 1996; 119 (Pt 4):1327–47. [PubMed: 8813295]

Martin MS, Dutt K, Papale LA, Dube CM, Dutton SB, de Haan G, et al. Altered function of the SCN1A voltage-gated sodium channel leads to gamma-aminobutyric acid-ergic (GABAergic) interneuron abnormalities. J Biol Chem. 2010; 285:9823–34. [PubMed: 20100831]

Medvedev AV. Temporal binding at gamma frequencies in the brain: paving the way to epilepsy? Australas Phys Eng Sci Med. 2001; 24:37–48. [PubMed: 11458571]

Mirnics K, Middleton FA, Marquez A, Lewis DA, Levitt P. Molecular characterization of schizophrenia viewed by microarray analysis of gene expression in prefrontal cortex. Neuron. 2000; 28:53–67. [PubMed: 11086983]

O'Roak BJ, Deriziotis P, Lee C, Vives L, Schwartz JJ, Girirajan S, et al. Exome sequencing in sporadic autism spectrum disorders identifies severe de novo mutations. Nat Genet. 2011; 43:585–9. [PubMed: 21572417]

Oakley JC, Kalume F, Yu FH, Scheuer T, Catterall WA. Temperature- and age-dependent seizures in a mouse model of severe myoclonic epilepsy in infancy. Proc Natl Acad Sci U S A. 2009; 106:3994–9. [PubMed: 19234123]

Ogiwara I, Miyamoto H, Morita N, Atapour N, Mazaki E, Inoue I, et al. Na(v)1.1 localizes to axons of parvalbumin-positive inhibitory interneurons: a circuit basis for epileptic seizures in mice carrying an Scn1a gene mutation. J Neurosci. 2007; 27:5903–14. [PubMed: 17537961]

Papale LA, Beyer B, Jones JM, Sharkey LM, Tufik S, Epstein M, et al. Heterozygous mutations of the voltage-gated sodium channel SCN8A are associated with spike-wave discharges and absence epilepsy in mice. Hum Mol Genet. 2009; 18:1633–41. [PubMed: 19254928]

Schwaller B, Tetko IV, Tandon P, Silveira DC, Vreugdenhil M, Henzi T, et al. Parvalbumin deficiency affects network properties resulting in increased susceptibility to epileptic seizures. Mol Cell Neurosci. 2004; 25:650–63. [PubMed: 15080894]

Scotti AL, Kalt G, Bollag O, Nitsch C. Parvalbumin disappears from GABAergic CA1 neurons of the gerbil hippocampus with seizure onset while its presence persists in the perforant path. Brain Res. 1997; 760:109–17. [PubMed: 9237525]

Sloviter RS, Zappone CA, Harvey BD, Bumanglag AV, Bender RA, Frotscher M. "Dormant basket cell" hypothesis revisited: relative vulnerabilities of dentate gyrus mossy cells and inhibitory

interneurons after hippocampal status epilepticus in the rat. J Comp Neurol. 2003; 459:44–76. [PubMed: 12629666]

Tang B, Dutt K, Papale L, Rusconi R, Shankar A, Hunter J, et al. A BAC transgenic mouse model reveals neuron subtype-specific effects of a Generalized Epilepsy with Febrile Seizures Plus (GEFS+) mutation. Neurobiol Dis. 2009; 35:91–102. [PubMed: 19409490]

van der Weyden L, Adams DJ, Harris LW, Tannahill D, Arends MJ, Bradley A. Null and conditional semaphorin 3B alleles using a flexible puroDeltatk loxP/FRT vector. Genesis. 2005; 41:171–8. [PubMed: 15789413]

Vawter MP, Crook JM, Hyde TM, Kleinman JE, Weinberger DR, Becker KG, et al. Microarray analysis of gene expression in the prefrontal cortex in schizophrenia: a preliminary study. Schizophr Res. 2002; 58:11–20. [PubMed: 12363385]

Wendling F, Bartolomei F, Bellanger JJ, Chauvel P. Epileptic fast activity can be explained by a model of impaired GABAergic dendritic inhibition. Eur J Neurosci. 2002; 15:1499–508. [PubMed: 12028360]

Woo TU, Walsh JP, Benes FM. Density of glutamic acid decarboxylase 67 messenger RNA-containing neurons that express the N-methyl-D-aspartate receptor subunit NR2A in the anterior cingulate cortex in schizophrenia and bipolar disorder. Arch Gen Psychiatry. 2004; 61:649–57. [PubMed: 15237077]

Yu FH, Mantegazza M, Westenbroek RE, Robbins CA, Kalume F, Burton KA, et al. Reduced sodium current in GABAergic interneurons in a mouse model of severe myoclonic epilepsy in infancy. Nat Neurosci. 2006; 9:1142–9. [PubMed: 16921370]

Highlights

- $Na_v1.1$ is expressed in most PV interneurons in the neocortex and hippocampus.
- $Na_v1.1$ is expressed in 5–13% of excitatory cells in neocortex and hippocampus.
- Preferential inactivation of one *Scn1a* allele in PV interneurons reduces seizure thresholds.
- Inactivation of one *Scn1a* allele in excitatory cells does not alter seizure thresholds.
- Preferential inactivation of one *Scn1a* allele in PV interneurons results in spontaneous seizures.

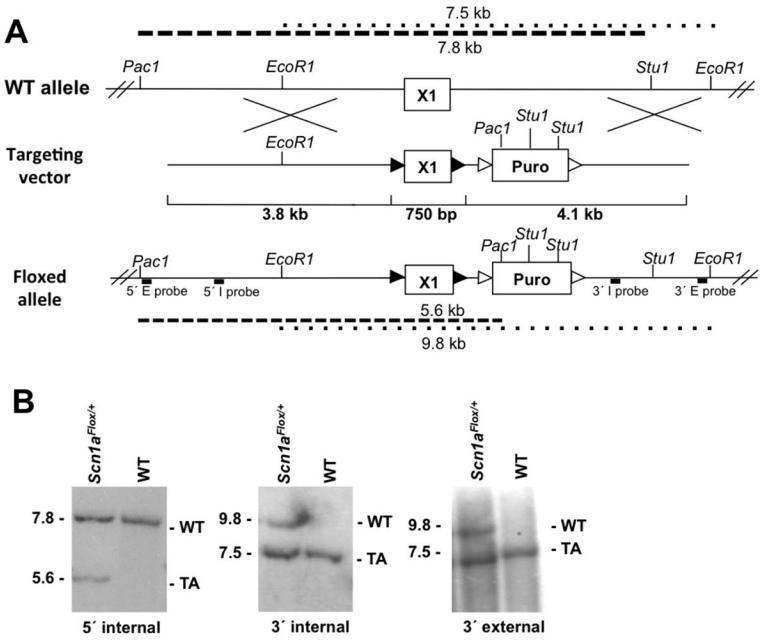

Figure 1. Targeting construct and generation of *Scn1a*$^{Flox/+}$ mice

(A) Diagram of the strategy used to generate the floxed *Scn1a* allele. Homologous recombination between the targeting construct and the endogenous *Scn1a* locus resulted in the floxed allele in which *Scn1a* exon 1 is flanked by two LoxP sequences. *Pac1*, *Stu1*, and *EcoR1* restriction sites, the location of probes for Southern blot analysis, and the lengths of the restriction fragments are shown. LoxP and FRT sites are represented by black and open triangles, respectively.

(B) Southern blot analysis of ES cell genomic DNA. After digestion with *Pac1/Stu1*, the 5′ internal probe (5′I) detected the predicted 7.8- and 5.6-kb fragments that correspond to the WT and *Scn1a*-floxed allele, respectively. Fragments of 9.8- and 7.5-kb from the WT and *Scn1a*-floxed allele, respectively, were detected with the 3′ internal (3′I) and 3′ external (3′E) probes following digestion with *EcoR1*. Dashed lines above figure, predicted restriction fragments from WT allele; dashed lines below figure, predicted restriction fragments from floxed allele.

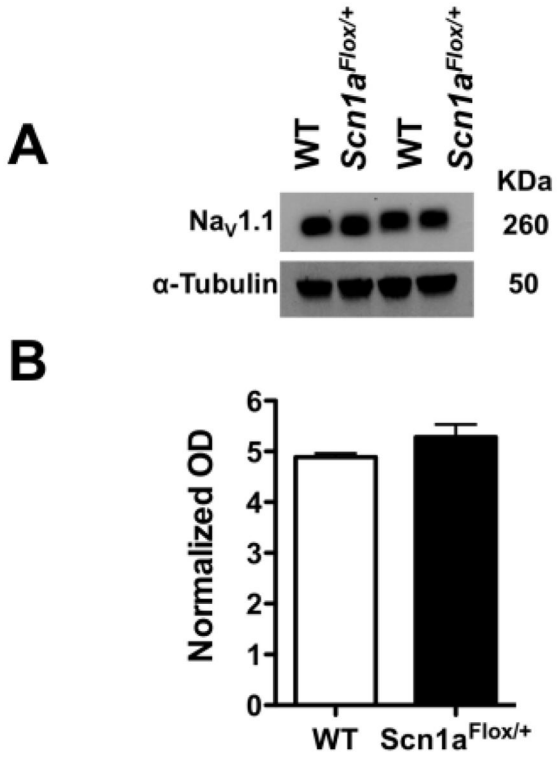

Figure 2. The floxed *Scn1a* allele does not alter $Na_V1.1$ protein levels

(A) Western blot analysis of whole brain membrane-bound proteins (25 μg) from P22 WT and *Scn1a*$^{Flox/+}$ mice shows the expected 260-KDa $Na_V1.1$ band. (B) Quantitative analysis of $Na_V1.1$ levels was performed on three separate Western blots. $Na_V1.1$ protein levels were normalized against α-tubulin as an internal control. OD, optical density. Error bars represent SEM.

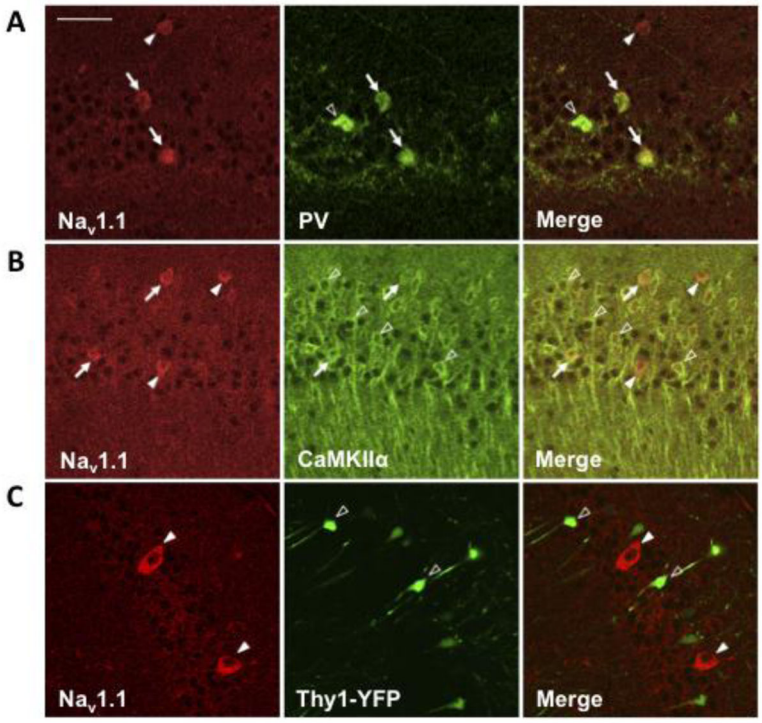

Figure 3. Co-localization of Na$_v$1.1 and cell-type markers in the hippocampus

(A) Extensive co-localization was observed between Na$_v$1.1 and PV immunoreactivity. (B) Thirteen percent of Na$_v$1.1-postive cells show *CaMK2α* immunoreactivity. (C) Only 1% of Na$_v$1.1-positive cells co-localize with Thy1-YFP-positive excitatory cells. The images in this figure are from the CA1 region of the hippocampus. Solid arrows, cells that are positive for Na$_v$1.1 and the cell-type marker; Solid arrowheads, Na$_v$1.1-positive cells that are negative for the respective cell-type marker; Open arrowheads, cells that are positive for the cell-type marker and are negative for Na$_v$1.1. Scale bar: 100μm.

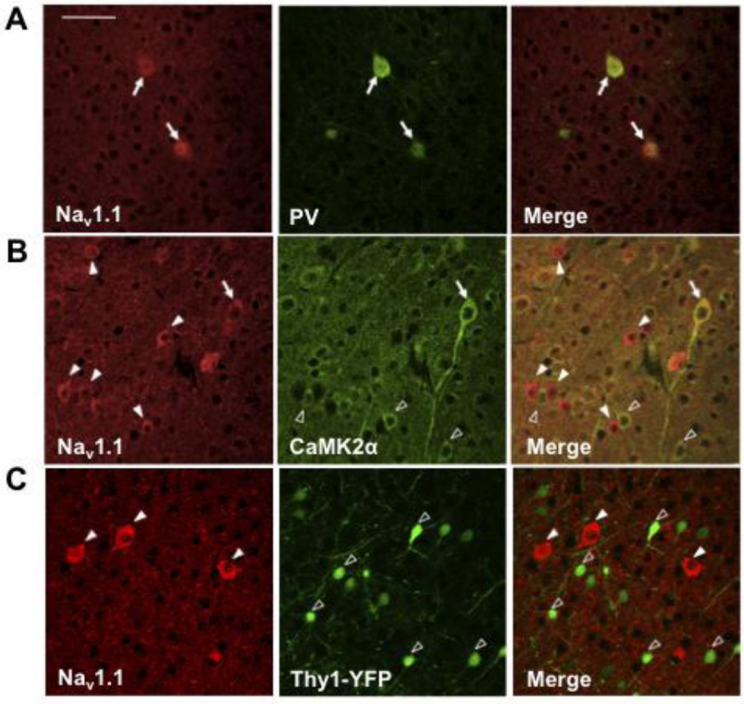

Figure 4. Co-localization of Na$_v$1.1 and cell-type markers in the neocortex

(A) Extensive co-localization between Na$_v$1.1 and PV immunoreactivity. (B) Five percent of cortical Na$_v$1.1-positive cells show *CaMK2α* immunoreactivity. (C) Na$_v$1.1 was not detected in Thy1-YFP-positive excitatory cells. Images are of layer 5 neocortical neurons. Arrows indicate co-localization between Na$_v$1.1 and the respective cell-type marker. Solid arrows, cells that are positive for Na$_v$1.1 and the cell-type marker; Solid arrowheads, Na$_v$1.1-positive cells that are negative for the respective cell-type marker; Open arrowheads, cells that are positive for the cell-type marker and are negative for Na$_v$1.1. Scale bar: 100μm.

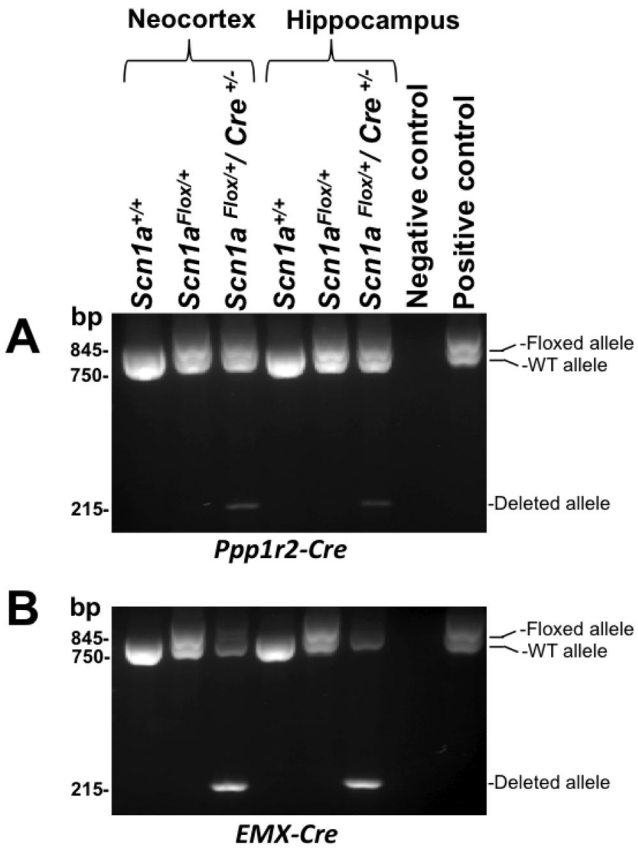

Figure 5. Confirmation of heterozygous *Scn1a* deletion in the neocortex and hippocampus

To confirm deletion of the floxed *Scn1a* allele in mice generated from the (A) *Ppp1r2-Cre* and (B) *EMX-Cre* crosses, PCR was performed on genomic DNA isolated from the hippocampus and neocortex of $Scn1a^{+/+}$, $Scn1a^{Flox/+}$, and $Scn1a^{Flox/+}/Cre^{+/-}$ mice. PCR products of 750- and 845-bp were generated from the WT and floxed alleles, respectively. The 215-bp PCR product confirmed the deletion of *Scn1a* exon 1 from the floxed allele.

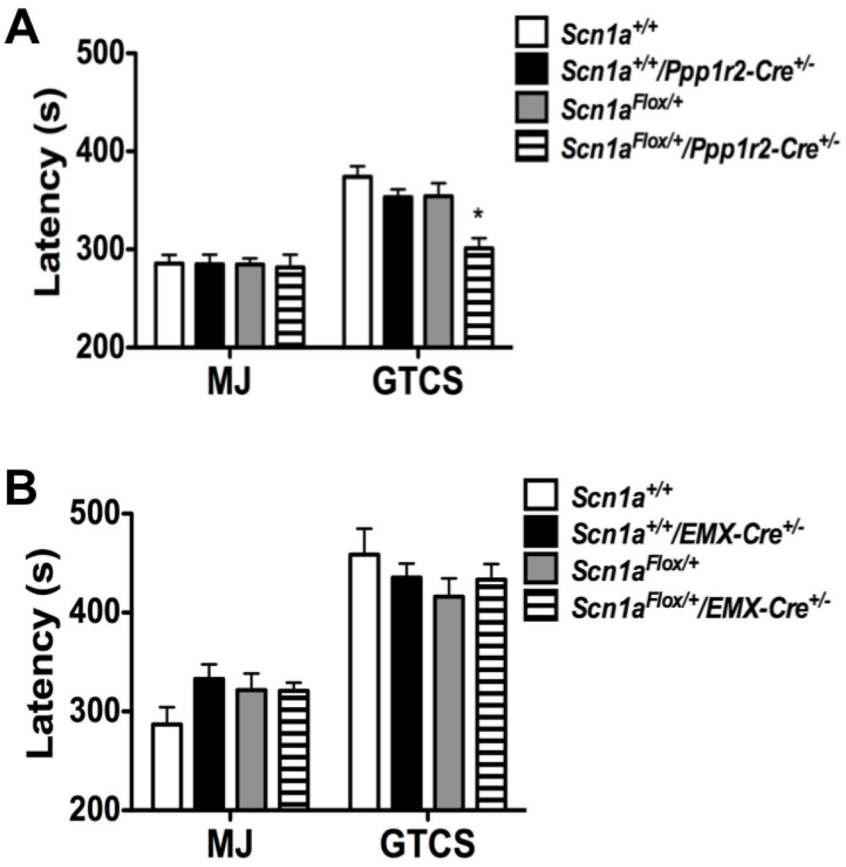

Figure 6. Preferential inactivation of *Scn1a* in PV interneurons results in reduced thresholds to flurothyl-induced seizures

Average latencies in seconds (s) to the MJ and GTCS after exposure to flurothyl in (A) *Scn1a*$^{Flox/+}$/*Ppp1r2-Cre*$^{+/-}$ mice and control littermates (n = 12 per genotype), and (B) *Scn1a*$^{Flox/+}$/*EMX-Cre*$^{+/-}$ mice and control littermates (n = 16–19 per genotype). There was no statistically significant difference in average latency to the MJ between *Scn1a*$^{Flox/+}$/*Ppp1r2-Cre*$^{+/-}$ mutants and control littermates; however, the average latency to the GTCS was significantly shorter in the mutants. No statistically significant differences in average latencies to the MJ and GTCS were observed between *Scn1a*$^{Flox/+}$/*EMX-Cre*$^{+/-}$ mice and control littermates. *, $p<0.05$, one-way analysis of variance (ANOVA). Error bars represent SEM.

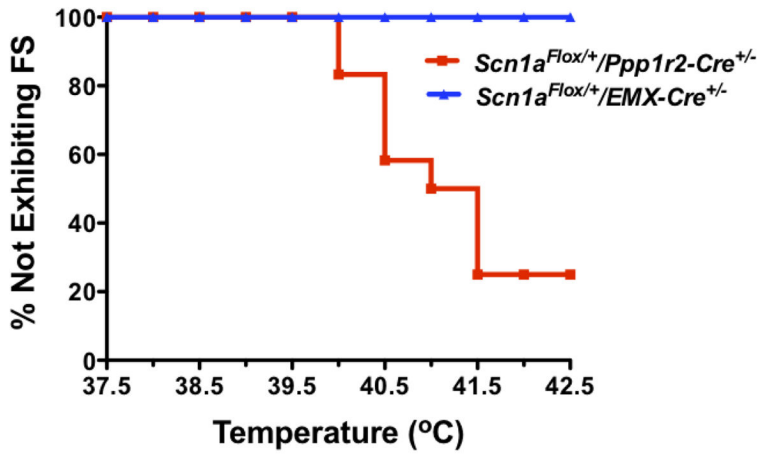

Figure 7. Preferential inactivation of *Scn1a* in PV interneurons results in increased susceptibility to hyperthermia-induced seizures

Hyperthermia-induced seizure thresholds were evaluated in P22 *Scn1a*$^{Flox/+}$, *Scn1a*$^{Flox/+}$/*Ppp1r2-Cre*$^{+/-}$ and *Scn1a*$^{Flox/+}$/*EMX-Cre*$^{+/-}$ mice. Twelve mice from each genotype were evaluated. Seizures were not observed in the *Scn1a*$^{Flox/+}$ or *Scn1a*$^{Flox/+}$/*EMX-Cre*$^{+/-}$ mice. The percentage of *Scn1a*$^{Flox/+}$/*Ppp1r2-Cre*$^{+/-}$ and *Scn1a*$^{Flox/+}$/*EMX-Cre*$^{+/-}$ mice not exhibiting seizures at each experimental temperature is shown. Seizures were induced in 75% of the *Scn1a*$^{Flox/+}$/*Ppp1r2-Cre*$^{+/-}$ mice at an average temperature of 40.7 ± 0.2.

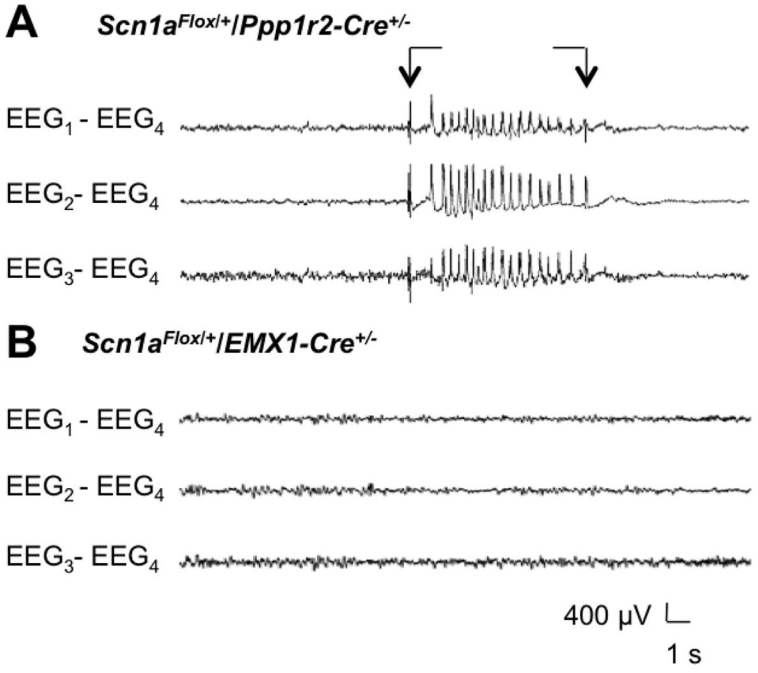

Figure 8. EEG confirmation of hyperthermia-induced seizures

Representative EEG traces of (A) Twenty-two day old *Scn1a*$^{Flox/+}$*/Ppp1r2-Cre*$^{+/-}$ mouse at the seizure-inducing temperature and (B) Twenty-two day old *Scn1a*$^{Flox/+}$*/EMX-Cre*$^{+/-}$ mouse at the maximum temperature of 42.5°C. Arrows indicate seizure onset and seizure termination in the *Scn1a*$^{Flox/+}$*/Ppp1r2-Cre*$^{+/-}$ mouse. No EEG abnormalities were observed in the *Scn1a*$^{Flox/+}$*/EMX-Cre*$^{+/-}$ mouse. EEG-EEG montage: Three cortical electrodes (EEG_1-EEG_3) with EEG_4 serving as the reference electrode. Calibration mark: 30 µV/mm and 1 second.

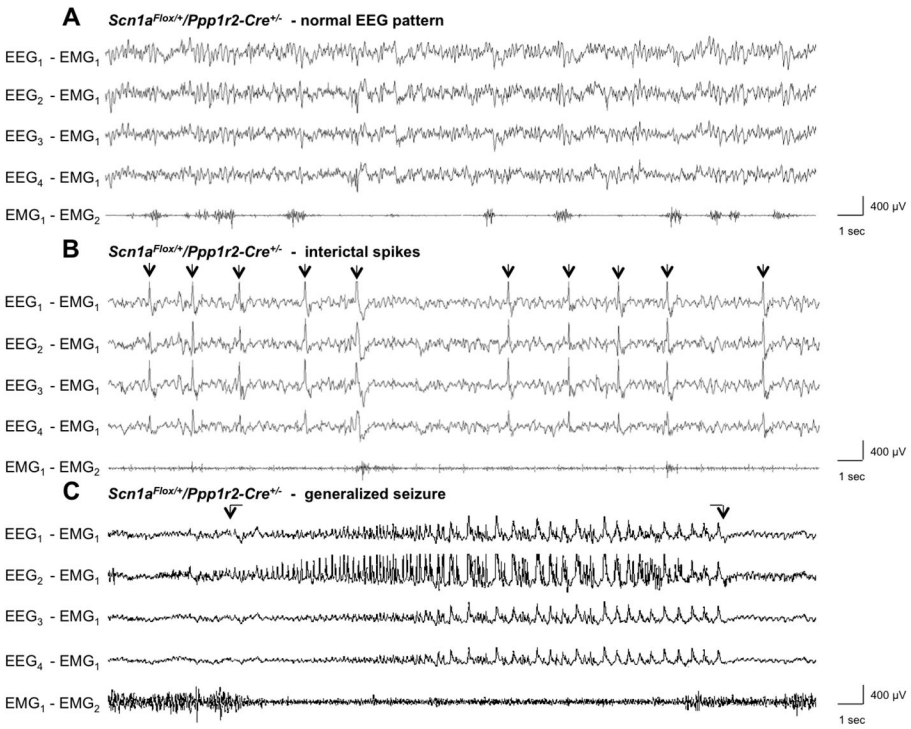

Figure 9. Spontaneous seizures following preferential inactivation of *Scn1a* in PV interneurons

(A) Normal EEG pattern from an awake *Scn1a*$^{Flox/+}$/*Ppp1r2-Cre*$^{+/-}$ mutant.

(B) High amplitude single spike discharges (arrows) observed in an *Scn1a*$^{Flox/+}$/*Ppp1r2-Cre*$^{+/-}$ mutant that were associated with jerking movements.

(C) Spontaneous generalized seizure in an *Scn1a*$^{Flox/+}$/*Ppp1r2-Cre*$^{+/-}$ mutant. High amplitude spike discharges were initially observed in the temporal region of the right hemisphere (channel EEG_2) with subsequent spread to all EEG channels (between arrows) and abrupt termination and return to normal waveforms. Note that increased muscle tone was observed prior to and following the seizure, indicating that this generalized seizure was associated with a lack of movement. EEG_1 and EEG_2, EEG recordings from the right cortical hemisphere; EEG_3 and EEG_4, EEG recordings from the left cortical hemisphere; EMG, electromyographic recording. EEG-EMG montage: four cortical electrodes referenced to the muscle electrode. EMG-EMG montage: both muscle electrodes referenced to each other. Calibration mark: 30 µV/mm and 1 second.